

**Citation:**

Mirabal, Nestor and Bonaca, Ana." Machine-Learned Dark Matter Subhalo Candidates in the 4FGL-DR2: Search for the Perturber of the GD-1 Stream." Journal of Cosmology and Astroparticle Physics, vol 2021 (15 November 2021). <https://doi.org/10.1088/1475-7516/2021/11/033>.

**DOI:**

<https://doi.org/10.1088/1475-7516/2021/11/033>

Access to this work was provided by the University of Maryland, Baltimore County (UMBC) ScholarWorks@UMBC digital repository on the Maryland Shared Open Access (MD-SOAR) platform.

**Please provide feedback**

Please support the ScholarWorks@UMBC repository by emailing [scholarworks-group@umbc.edu](mailto:scholarworks-group@umbc.edu) and telling us what having access to this work means to you and why it's important to you. Thank you.

# Machine-Learned Dark Matter Subhalo Candidates in the 4FGL-DR2: Search for the Perturber of the GD-1 Stream

Nestor Mirabal<sup>a,b,c</sup> Ana Bonaca<sup>d</sup>

<sup>a</sup>Mail Code 661, Astroparticle Physics Laboratory, NASA Goddard Space Flight Center, Greenbelt, MD 20771, USA

<sup>b</sup>University of Maryland, Baltimore County, MD 21250, USA

<sup>c</sup>Center for Research and Exploration in Space Science and Technology, NASA Goddard Space Flight Center, Greenbelt, MD 20771

<sup>d</sup>Center for Astrophysics | Harvard & Smithsonian, 60 Garden Street, Cambridge, MA 02138, USA

E-mail: [nestor.r.mirabalbarrios@nasa.gov](mailto:nestor.r.mirabalbarrios@nasa.gov), [ana.bonaca@cfa.harvard.edu](mailto:ana.bonaca@cfa.harvard.edu)

**Abstract.** The detection of dark matter subhalos without a stellar component in the Galactic halo remains a challenge. We use supervised machine learning to identify high-latitude gamma-ray sources with dark matter-like spectra among unassociated gamma-ray sources in the 4FGL-DR2. Out of 843 4FGL-DR2 unassociated sources at  $|b| \geq 10^\circ$ , we select 73 dark matter subhalo candidates. Of the 69 covered by the *Neil Gehrels Swift Observatory* (*Swift*), 17 show at least one X-ray source within the 95% LAT error ellipse and 52 where we identify no new sources. This latest inventory of dark subhalos candidates allows us to investigate the possible dark matter substructure responsible for the perturbation in the GD-1 stellar stream. In particular, we examine the possibility that the alleged GD-1 dark subhalo may appear as a 4FGL-DR2 gamma-ray source from dark matter annihilation into Standard Model particles.

---

## Contents

<b>1</b>	<b>Introduction</b>	<b>1</b>
<b>2</b>	<b>Dark Subhalo Selection</b>	<b>2</b>
2.1	Dataset	2
2.2	Machine Learning Algorithms	3
2.3	Feature Selection	3
2.4	Training and Classification	4
<b>3</b>	<b>X-ray Observations</b>	<b>5</b>
<b>4</b>	<b>Searching for the GD-1 Perturber</b>	<b>6</b>
<b>5</b>	<b>Is GD-1’s Perturbing Subhalo Detectable in Gamma Rays?</b>	<b>7</b>
<b>6</b>	<b>They Might Be Pulsars</b>	<b>8</b>
<b>7</b>	<b>Conclusions and Future Work</b>	<b>8</b>

---

## 1 Introduction

It has been long hypothesized that the Milky Way halo is populated by thousands of dark matter subhalos above a mass of  $10^6 M_\odot$  [1–3]. With dedicated optical surveys, the number of detected dwarf galaxies orbiting the Milky Way has grown significantly and sets a lower bound on the abundance of dark matter subhalos [4]. However, there might be dark substructures that are too faint or too distant to be picked up by optical surveys alone [5]. Localizing dark matter subhalos without detectable stellar populations is still of critical importance not only to understand structure formation but also to reveal the particle nature of dark matter directly.

Weakly interacting massive particles (WIMPs) in the nearest and most massive subhalos could produce observable gamma-ray sources with significantly curved energy spectra from annihilating dark matter [6]. In general, one can parametrize WIMP annihilation spectra with a super-exponential cutoff power law [7, 8]:

$$\frac{dN_{DM}}{dE}(E) = K \left( \frac{E}{E_0} \right)^{-\Gamma} e^{-\left( \frac{E}{E_{cut}} \right)^\beta}, \quad (1.1)$$

where  $K$  is a prefactor,  $E_0 = 10^3$  MeV is the pivot energy,  $\Gamma$  is the spectral photon index,  $E_{cut}$  is the cutoff energy and  $\beta$  is the curvature index. Taking advantage of the extraordinary map of the gamma-ray sky produced by the Large Area Telescope (LAT) on the *Fermi Gamma-ray Space Telescope* (*Fermi*), several searches have used source catalogs released by the LAT collaboration to look for this distinctive spectral feature among unassociated sources [7–19]. Although there are interesting subhalo candidates with exponential cutoffs, it is still not yet possible to distinguish them from gamma-ray pulsars [16].

An alternate approach is based on the idea that dark matter subhalos orbiting in the Milky Way halo might induce gaps when they cross elongated dynamically-cold stellar streams

[20–24]. With astronomical surveys such as the *Gaia* mission, there is now sufficient precision to study stellar streams in extreme detail. The GD-1 stellar stream is currently the most notable example of a possible stream crossing [25, 26]. The observed morphology of GD-1 (gap and off-stream spur of stars) is naturally reproduced in models of the stellar stream that include an encounter with a massive object ( $\sim 10^6 - 10^8 M_\odot$ ), like a globular cluster, a dwarf galaxy, or a dark matter subhalo [26, 27].

Each of these techniques offers excellent opportunities to survey the subhalo population. But a combination of approaches might boost our chances for success. In this paper, we use the first incremental version of the Fourth *Fermi*-LAT Catalog of gamma ray sources (4FGL-DR2, for Data Release 2) to select possible dark matter subhalos using machine-learning techniques [12, 18]. Out of 843 unassociated gamma-ray sources at  $|b| \geq 10^\circ$ , we extract a subset of 73 sources that are consistent with the spectral shape of annihilating dark matter. We then search for X-ray sources in the LAT 95% error ellipses using archival *Swift* data. We next compare the locations of the subhalo candidates with the predicted locations of the GD1’s perturbing subhalo from *Gaia*.

## 2 Dark Subhalo Selection

### 2.1 Dataset

We start with the 4FGL-DR2 covering the time period August 4, 2008, to August 2, 2018 in the 50 MeV-1 TeV energy range [28, 29]. For our study, we use the latest version available at the time of this writing `gll-psc-v27.fit`. These sources are extremely well characterized by 74 catalog columns. Of the 5787 4FGL-DR2 sources, 1670 are unassociated. This leaves 4117 associated sources. Since we are only interested in searching for dark subhalo candidates away from the Galactic plane, we can safely remove Galactic plane sources such as supernova remnants and pulsar wind nebulae. The largest source population at high Galactic latitude is extragalactic. We parametrize these sources with an extragalactic set that includes 3505 training sources from all AGN classes in the 4FGL. The extragalactic set includes 11 non-blazar active galaxies (AGN,agn), 1382 blazar candidates of uncertain type (BCU,bcu), 1308 BL Lacs (BLL,bl), 743 flat-spectrum radio quasars (FSRQ,fsrq), 9 narrow-line Seyferts 1 (NLSY1,nlsy1), 44 radio galaxies (RDG,rdg), 2 soft spectrum radio quasars (ssrq), 5 compact steep spectrum quasar (css), and 1 Seyfert galaxy (sey).

In order to generate a model for dark subhalo searches we harness the vast catalog of gamma-ray pulsar and globular cluster spectra [18]. Early studies of unassociated gamma-ray sources led to the important realization that gamma-ray pulsar spectra would be nearly indistinguishable from the super-exponential spectra generated by WIMP annihilation in dark subhalos [6]. Thus formally, a high-latitude, non-variable gamma-ray pulsar candidate without detected pulsation is also a potential subhalo candidate. For our subhalo set, we include 235 identified pulsars (PSRs), 30 globular clusters (glc), and 24 associated pulsars (psrs) with spectra that are also consistent with annihilations of  $\sim 20$ –70 GeV dark matter particles [16, 17].

We end up with a grand total of 3794 training sources. With 3505 extragalactic and 289 pulsars, our training set is imbalanced. Whenever there is imbalance, machine learning classification tends to be artificially skewed towards the majority class. As in [18], we use the Synthetic Minority Over-sampling Technique to balance the class distribution (SMOTE, [30]). SMOTE adds synthetic pulsars sampled from the existing pulsars using  $k$ -nearest neighbors until they both contain near equal samples.

## 2.2 Machine Learning Algorithms

For 4FGL-DR2 training, testing and classification, we rely on the scheme introduced in [18]. For training we use Random Forest and eXtreme Gradient Boosting (XGBoost) tree algorithms. Although both rely on classification trees, Random Forest uses feature bagging that makes decisions by a committee of individual classification trees. Each tree casts a vote for the predicted class and the majority vote is taken as the prediction, thus it reduces variance [31]. XGBoost <sup>1</sup> tries to do better at each interaction, thus it reduces bias [32]. We settle on a combination of R and **scikit-learn** <sup>2</sup> for the rest of the paper.

## 2.3 Feature Selection

Given the large number of 4FGL-DR2 features, it is critical to determine their relative importance for correct classification. To do this we rely on the Gini coefficient as determined by Random Forest [33, 34]. A larger value of Gini importance means that a particular feature plays a greater role in predicting a certain class. This is shown in Figure 1. As shown, the most important predictors are:

- **LP\_SigCurv**: Significance (in  $\sigma$  units) of the fit improvement between PowerLaw and LogParabola.
- **PLEC\_SigCurv**: Same as LP\_SigCurv for PLSuperExpCutoff model
- **LP\_beta**: Curvature parameter when fitting with LogParabola
- **Flux1000**: Integral photon flux from 1 to 100 GeV
- **Frac\_Variability**: Fractional variability computed from the fluxes in each year
- **Variability\_Index**: Sum of  $2 \times \log(\text{Likelihood})$  difference between the flux fitted in each time interval and the average flux over the full catalog interval
- **PLEC\_Index**: Low-energy photon index when fitting with PLSuperExpCutoff
- **PL\_Index**: Photon index when fitting with PowerLaw
- **Pivot\_Energy**: Energy at which error on differential flux is minimal
- **LP\_Index**: Photon index at Pivot Energy when fitting with LogParabola

Another reliable importance measure is the evaluation of “out-of-bag” (OOB) performance as a function of number of features. As can be seen Figure 1, the OOB performance tends to settle after 8 or more features are included. Since there is no obvious learning loss, we decided to retain the top 10 features for the rest of the classification.

---

<sup>1</sup><https://github.com/dmlc/xgboost>

<sup>2</sup><http://www.scikit-learn.org>

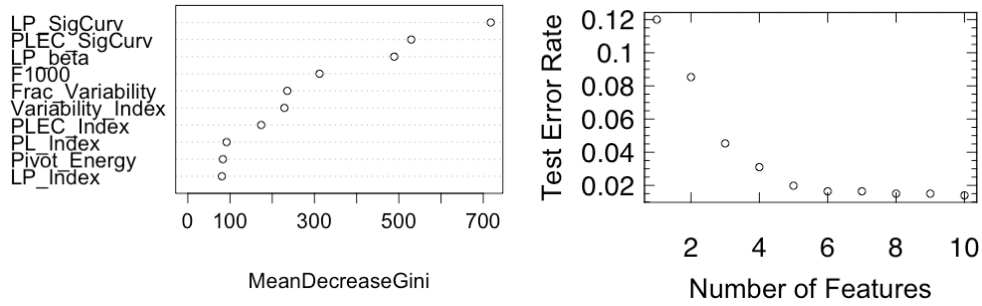


**Figure 1.** Left: Importance of the 10 top features that were used to train the Random Forest classifier. Right: Out-of-bag performance as a function of the number of features used by the classifier.

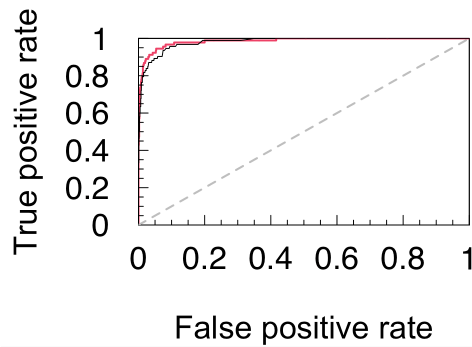


**Figure 2.** ROC curve comparison of the two methods. The red thick line shows XGBoost while the black thin line shows the curve for Random Forest.

## 2.4 Training and Classification

For cross validation, we divide the dataset into training (70%) and testing (30%) subsets. Overall, the Random Forest classifier achieves an accuracy of 97.7%. Similarly, XGboost reaches an accuracy of 97.4%. The fluidity of ongoing source association efforts offers another kind of sanity check. As our work evolved from the initial `gll-psc-v23.fit` 4FGL-DR2 file release to the current `gll-psc-v27.fit` version<sup>3</sup>, five of our machine-learned subhalo candidates moved from unassociated to pulsar associations<sup>4</sup> and are no longer included here. Figure 2 compares the Receiver Operating Characteristic curves (ROC curve) for the two methods. ROC curves allows us to visualize the True Positive Rate (sensitivity) against False Positive Rate (specificity). Curves closer to the top-left corner indicate a better performance.

Having trained the classifiers using labeled LAT sources, we can now identify dark subhalo candidates among unassociated 4FGL-DR2 sources. To cut back on contamination from Galactic plane objects, we only use unassociated sources at high latitude ( $|b| \geq 10^\circ$ ). After data cleaning, we end up with 843 unassociated sources at  $|b| \geq 10^\circ$ . Applying our machine-learning models to this sample, we end up with 73 4FGL-DR2 sources which both our methods predict to be dark subhalos. Table 1 presents the list of sources consistent with being subhalo candidates. Figure 3 shows their location in RA-Dec (top) and Galactic (bottom) coordinates.

<sup>3</sup>[https://fermi.gsfc.nasa.gov/ssc/data/access/lat/10yr\\_catalog/](https://fermi.gsfc.nasa.gov/ssc/data/access/lat/10yr_catalog/)

<sup>4</sup>4FGL J0312.1–0921, 4FGL J1221.4–0634, 4FGL J1304.4+1203, 4FGL J1400.6–1432, 4FGL J2039.4–3616

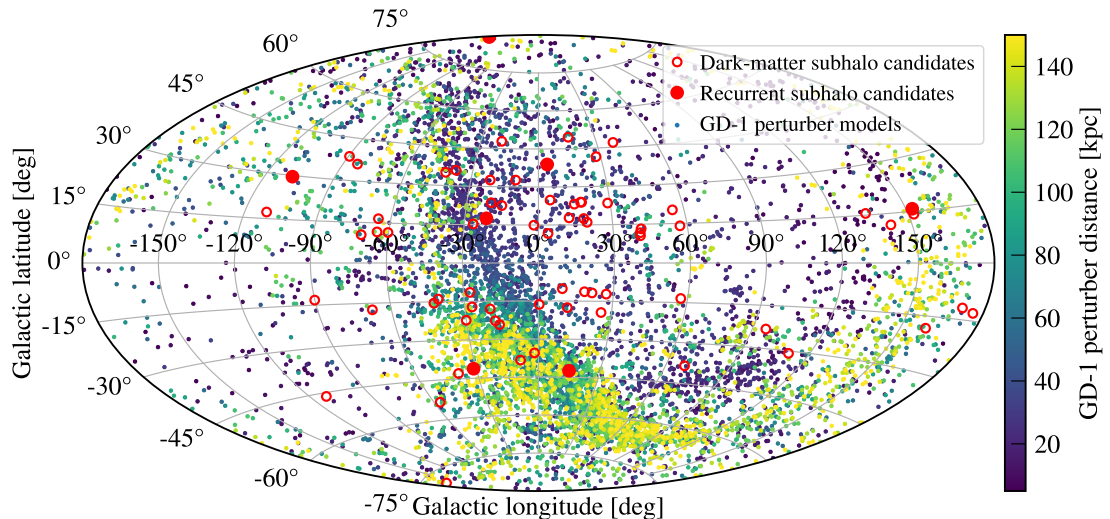


**Figure 3.** Locations of 73 dark subhalo candidates in the Galactic sky coordinates (empty red circles). Candidates recurring in multiple *Fermi* data releases are marked as solid red circles. The color-coded dots indicate the predicted distance of the GD-1 perturbing subhalo.

### 3 X-ray Observations

For each source in Table 1, we select all observations available in the *Swift* archive. The majority are part of a long-term follow-up program of unassociated *Fermi* sources [35]. In total, we find that 69 of the 73 sources have had their 95% error ellipse covered. For the X-ray Telescope (XRT) analysis, we used XRTDAS<sup>5</sup> within HEASOFT 6.26. We used the standard selections of 0 – 12 in the Photon Counting (PC) mode and performed the analyses in the 0.3–10 keV energy range. In case of a point source detection within the 95% error ellipse, we extract the number of photons from a circular region around the source with radius 20 arcseconds and a 40–150 arcsecond annular region to describe the background and scale it to the source region. In total, 17 4FGL-DR2 sources show one or more X-ray detections within their 95% error ellipse. Whenever there is a detection, X-ray fluxes are calculated assuming photon index 2 and the full Galactic  $N_{\text{H}}$  estimated using WebPIMMS<sup>6</sup>. See Table 2 for flux values.

In order to place X-ray upper limits, we followed a procedure similar to [36]. We extract the number of photons from the brightest circular region within the LAT 95% ellipse. Using annular background regions, we compute the expected number of background photons and compute the 90% confidence lower limit in the background region [37]. The upper limit is derived by subtracting this lower limit from the observed photons in the source region. To determine upper limits for nondetections, we assume an absorbed power law with photon index 2 and  $N_{\text{H}}$  from WebPIMMS. Results are listed in Table 1. In order to double check our results, we used the online *Swift* XRT products generator<sup>7</sup> based on tools developed for the 2SXPS *Swift* XRT Point Source Catalogue [38]. Finally, we also consulted the online version of the *Swift*-XRT Survey of *Fermi* Unassociated Sources program for consistency<sup>8</sup>.

<sup>5</sup>[https://swift.gsfc.nasa.gov/analysis/xrt\\_swguide\\_v1\\_2.pdf](https://swift.gsfc.nasa.gov/analysis/xrt_swguide_v1_2.pdf)

<sup>6</sup><https://heasarc.gsfc.nasa.gov/cgi-bin/Tools/w3pimms/w3pimms.pl>

<sup>7</sup><https://www.swift.ac.uk/>

<sup>8</sup><https://www.swift.psu.edu/unassociated/>



## 4 Searching for the GD-1 Perturber

Searches for low-mass dark-matter subhalos in the Milky Way galaxy focus on detecting their effects on the motions of halo stars. Stellar streams are especially sensitive tracers of such low-amplitude gravitational perturbations [39, 40]. Formed by tidal dissolution of a progenitor star cluster or dwarf galaxy, stellar streams are long, thin and kinematically cold groups of stars moving on similar orbits through the Galaxy for billions of years [41–43]. A subhalo passing by a stellar stream imparts measurable velocity kicks to its member stars. Less massive subhalos merely increase the stream’s velocity dispersion [39], while more massive ones significantly alter stellar orbits to produce an underdensity, or a “gap”, in the stellar stream [23]. Parameters of the impact, including the subhalo mass and time of impact, remain recorded in the density and kinematic structure of the perturbed region [44, 45]. Early analyses of photometric data from the Sloan Digital Sky Survey (SDSS) revealed an abundance of stream gaps consistent with perturbation by a population of CDM subhalos [46, 47]. However, deeper photometry indicates that at least some of these density variations may be due to contamination from other Milky Way stars [48], rendering the detection of dark-matter subhalos with streams inconclusive in SDSS.

Proper motions provided by the *Gaia* mission vastly improved the selection of stream member stars. Applied to the GD-1 stellar stream, this selection revealed significant gaps in the stream density, as well as a spur of stream stars beyond the main stream track [49]. Numerical experiments show that a recent ( $\approx 0.5$  Gyr) impact of a massive ( $10^6 M_\odot - 10^8 M_\odot$ ) and compact ( $\lesssim 20$  pc) object can produce features observed in GD-1 [26]. Even though a spur-like structure can be induced in GD-1 by the Sagittarius dwarf galaxy [27], orbital integrations in the fiducial model of the Milky Way show that none of the known objects like dwarf galaxies, globular clusters, and molecular clouds, approach GD-1 sufficiently close to reproduce the structure of the GD-1 gap-and-spur features in detail [26]. This allows the possibility that GD-1 encountered a low-mass dark-matter subhalo.

The most direct way to ascertain the nature of a stream perturber would be to observe it directly. Detailed spatial distribution (the location and size of the observed gap and spur features) and kinematics (small radial velocity offset detected between the stream and spur) of the perturbed region of GD-1 constrain the perturber’s orbit [26]. Present-day sky positions of perturbers on allowed orbits are shown in Figure 3 and color-coded by their distance from the Sun (darker colors for more nearby models). *Fermi* dark-matter subhalo candidates are overplotted as large red circles. The present-day positions of the GD-1 perturber were calculated assuming an axisymmetric, static, analytic model of the Milky Way’s gravitational potential, whereas the most recent dynamical studies suggest that the halo shape is spatially complex and still evolving due to ongoing mergers with Sagittarius and Large Magellanic Cloud [50, 51]. Therefore, each individual perturber position is likely associated with a systematic uncertainty stemming from an overly simplified Milky Way model. Still, positions of a number of subhalo candidates overlap the general area plausibly occupied by the GD-1 perturber and provide valuable targets for follow-up observations.

Interestingly, the distribution of *Fermi* subhalo candidates is asymmetric with respect to the Galactic center: most candidates are located at Galactic latitudes  $|b| \lesssim 45^\circ$ , but with a larger extension to negative Galactic longitudes,  $-100^\circ \lesssim l \lesssim 60^\circ$ . Even more strikingly, the preferred sky positions of the GD-1 perturber are along a great circle. Dynamically, their orbits appear to be aligned with the orbital plane of the Sagittarius dwarf galaxy [26]. The robustness of these asymmetries needs to be further tested, e.g., with a more comprehensive



search of the orbital parameter space in the case of the GD-1 perturber, and with a more detailed accounting of *Fermi* sensitivity to subhalo signals. If confirmed, the asymmetric distribution of subhalo candidates suggests that at least a fraction of dark matter in the Milky Way is unrelaxed and that coherent debris flows from recent mergers [e.g., 51–54] need to be accounted for in studies of dark matter on Galactic scales.

## 5 Is GD-1’s Perturbing Subhalo Detectable in Gamma Rays?

To start answering this question, we must rely on cosmological simulations and  $J$  factor predictions. The expected gamma-ray flux from dark matter annihilation [55] is given by:

$$\frac{d\phi(\Delta\Omega)}{dE_\gamma} = \left( \frac{1}{4\pi} \frac{dN_\gamma}{dE_\gamma} \frac{\langle\sigma v\rangle}{2m_{DM}^2} \right) \left( \int_{\Delta\Omega} d\Omega \int_{\text{l.o.s.}} d\ell \rho_\chi^2(\vec{\ell}) \right). \quad (5.1)$$

The left term within parentheses represents the particle physics contribution where  $\langle\sigma v\rangle$  is the velocity-averaged annihilation cross section,  $m_{DM}$  is the WIMP mass, and  $dN_\gamma/dE_\gamma$  is the differential spectrum of gamma rays from annihilation of a pair of DM particles. The right hand side term (as shown in parentheses) represents the  $J$ -factor  $J$ , which encloses all the astrophysical considerations. The first integral is performed over the solid angle of a region of interest (ROI,  $\Delta\Omega$ ). The second integration is performed along the line of sight, and  $\rho(\vec{\ell})$  is the density of the DM particles.

Finding astronomical objects that maximize  $J$  is key to achieving a detection. Using predictions from the Via Lactea II [2] dark-matter only simulation, [8] find significantly higher  $J$ -factors associated to low-mass subhalos. With respect to previous works, [8] assigns “proper” subhalo concentrations and repopulated the VL-II simulations with low-mass subhalos down to  $10^3 M_\odot$ . The main limitation in these results is the unknown impact of baryons in the subhalo population.

Possibly the most careful job assessing the gamma-ray detectability of dark matter subhalos taking into account baryons and uncertainties in different cosmological simulations is by [56]. Using a set of four configurations including *Aquarius*, *Phat-ELVIS*, *Stref* and *Laval*, [56] find that there should be anywhere between 4 and 50 subhalos in the  $\sim 10^6 - 10^8 M_\odot$  mass range detectable in the 3FGL catalog between 15 kpc and 160 kpc. Relative to the 3FGL catalog, the 4FGL-DR2 used in this work has twice as much exposure.

Assuming a massive  $\sim 10^6 - 10^8 M_\odot$  perturbing subhalo (as in the previous section) and a 100 GeV dark matter particle annihilating to  $b\bar{b}$  at the thermal relic cross section, we expect a  $5\sigma$  significance detection of any subhalo with  $J \sim 10^{17.2} \text{ GeV}^2 \text{ cm}^{-5}$  within 8 kpc [57]. If  $J$  factors scale as the square of the distance to the target, one could detect subhalos with  $J \sim 10^{19.4} \text{ GeV}^2 \text{ cm}^{-5}$  out to 100 kpc. From our predicted distance of the perturbing subhalo, we find a wide distribution that would cover that detection range.

To substantiate these estimates, we use the **CLUMPY** code<sup>9</sup> to reproduce a scaled down version of  $J$ -factor predictions here. We follow a nearly identical approach as the one used in [58]. We generate subhalo sets ranging from  $m_{\min} = 10^{-6} M_\odot$  to  $m_{\max} = 0.01 M_{\text{tot}}$  using the default value for **CLUMPY** parameters. We assume a halo mass distribution  $dN/dm \propto m^{-\alpha_m}$  with  $\alpha_m = 1.9$  and set a limit of 150 subhalos between  $10^8 M_\odot$  and  $10^{10} M_\odot$ . An Einasto profile is the default configuration for the subhalo profile. In Figure 4, we show the brightest 2500 subhalos in 5 realizations at high Galactic latitude ( $|b| \geq 10^\circ$ ). As expected, we find

---

<sup>9</sup><https://clumpy.gitlab.io/CLUMPY/>

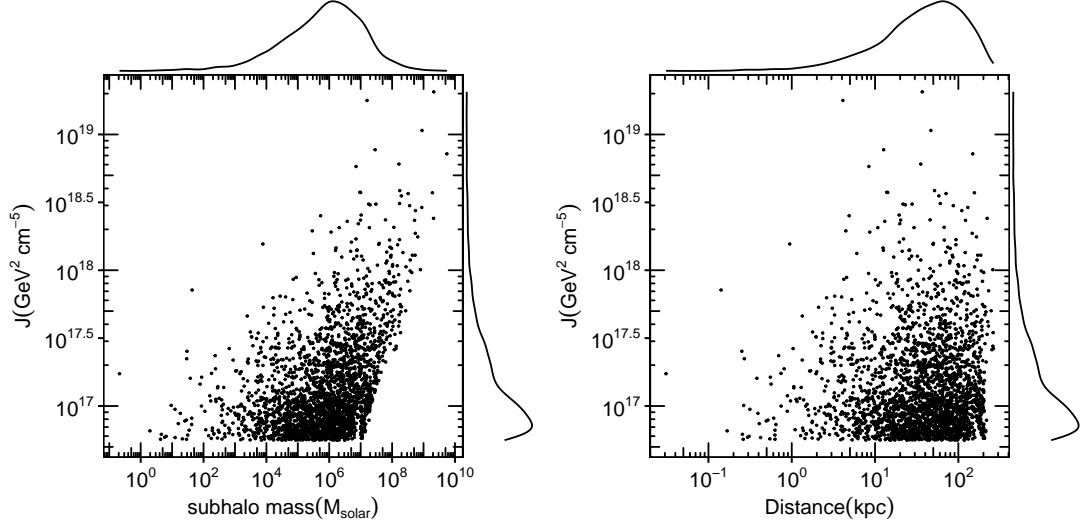


**Figure 4.** Left: Subhalo  $J$  factor as a function of subhalo mass. The points correspond to the 2500 brightest subhalos in 5 CLUMPY realizations. Right: Scatter plot of subhalo  $J$  factors as a function of distance from Earth for the same sample. Marginal density plot are also shown.

some of the largest  $J$ -factors in the  $\sim 10^6 - 10^8 M_\odot$  subhalo mass range within distances between 1 and 100 kpc. For a complete analysis using 500 simulations and a more complete discussion of CLUMPY caveats see [58].

## 6 They Might Be Pulsars

Throughout our discussion, we have noted that it might not be possible to distinguish between subhalos from annihilating  $\sim 20-70$  GeV dark matter particles and gamma-ray pulsars using spectral information alone. Based on population syntheses of millisecond pulsars, some models predict that *Fermi* could detect around 170 MSPs within 10 years [59]. As of this writing, there are 118 MSPs in the Public List of LAT-Detected Gamma-Ray Pulsars<sup>10</sup>. The upcoming Third *Fermi* LAT Pulsar Catalog (3PC in preparation) [60] will significantly expand the census of gamma-ray pulsars and facilitate a proper comparison with the list of candidates presented here.

## 7 Conclusions and Future Work

We present a list of 73 4FGL-DR2 sources that appear to be promising dark matter subhalo candidates. Out of the 69 covered by *Swift*, 17 show at least one X-ray source within the LAT ellipse. If we only consider gamma-ray sources detected in more than one catalog (1FGL, 2FGL, 3FGL, 4FGL, 4FGL-DR2), one can narrow the list further to 40 sources. From the analysis presented here and recurrent selection as subhalo candidates in previous works [8, 18, 61], we highlight a subset of seven sources that should be further investigated as potential subhalo candidates: 4FGL J0545.7+6016, 4FGL J0953.6-1509, 4FGL J1225.9+2951, 4FGL J1539.4-3323, 4FGL J1543.6-0244, 4FGL J2112.5-3043, and 4FGL J2133.1-6432. Out

<sup>10</sup><https://confluence.slac.stanford.edu/display/GLAMCOG/Public+List+of+LAT-Detected+Gamma-Ray+Pulsars>

of these seven candidates, 4FGL J1539.4-3323 and 4FGL J2112.5-3043 lie in sky locations with the highest density of allowed GD-1 perturber models with predicted distances smaller than 40 kpc.

It is important to note that the presumed subhalo spectra from annihilating  $\sim 20$ –70 GeV dark matter particles is consistent with the intriguing Galactic Center signal [62, 63]. Now there are two general caveats when interpreting our results. First, any correspondence between simulations and 4FGL-DR2 subhalo locations as in Figure 3 should not be taken directly as a distance proxy. Second, the mere presence of X-ray point sources within a LAT 95% error ellipse does not necessarily translate into an actual source association [28]. However, X-ray sources can provide initial follow-up targets for optical spectroscopy.

As the characterization of stellar streams improves, it might be possible to actually pinpoint the exact location of dark matter perturbing subhalos directly. This will further narrow down the potential gamma-ray counterpart. This work is a first attempt at what might be possible to achieve in the future.

## Acknowledgments

The material is based upon work supported by NASA under award number 80GSFC21M0002. This research has made use of data obtained through the High Energy Astrophysics Science Archive Research Center Online Service, provided by the NASA/Goddard Space Flight Center. This work made use of data supplied by the UK Swift Science Data Centre at the University of Leicester. We acknowledge valuable conversations with Javier Coronado-Blázquez. We thank Miguel Ángel Sánchez-Conde for providing many helpful comments on the entire manuscript. We also thank the referee for providing helpful comments. AB acknowledges support from NASA through HST grant HST-GO-15930.

## References

- [1] A. Klypin, A. V. Kravtsov, O. Valenzuela and F. Prada, *Where Are the Missing Galactic Satellites?*, *Astrophysical Journal* **522** (Sept., 1999) 82–92.
- [2] J. Diemand, M. Kuhlen and P. Madau, *Dark Matter Substructure and Gamma-Ray Annihilation in the Milky Way Halo*, *The Astrophysical Journal* **657** (Mar., 2007) 262–270, [[astro-ph/0611370](#)].
- [3] V. Springel, J. Wang, M. Vogelsberger, A. Ludlow, A. Jenkins, A. Helmi et al., *The Aquarius Project: the subhaloes of galactic haloes*, *Monthly Notices of the RAS* **391** (Dec., 2008) 1685–1711, [[0809.0898](#)].
- [4] J. D. Simon, *The Faintest Dwarf Galaxies*, *Annual Review of Astronomy and Astrophysics* **57** (Aug., 2019) 375–415, [[1901.05465](#)].
- [5] J. Zavala and C. S. Frenk, *Dark Matter Haloes and Subhaloes*, *Galaxies* **7** (Sept., 2019) 81, [[1907.11775](#)].
- [6] E. A. Baltz, J. E. Taylor and L. L. Wai, *Can Astrophysical Gamma-Ray Sources Mimic Dark Matter Annihilation in Galactic Satellites?*, *Astrophysical Journal Letters* **659** (Apr., 2007) L125–L128, [[astro-ph/0610731](#)].
- [7] F. Calore, V. De Romeri, M. Di Mauro, F. Donato and F. Marinacci, *Realistic estimation for the detectability of dark matter subhalos using Fermi-LAT catalogs*, *Physical Review D* **96** (Sept., 2017) 063009, [[1611.03503](#)].

- [8] J. Coronado-Blázquez, M. A. Sánchez-Conde, A. Domínguez, A. Aguirre-Santaella, M. Di Mauro, N. Mirabal et al., *Unidentified gamma-ray sources as targets for indirect dark matter detection with the Fermi-Large Area Telescope*, *Journal of Cosmology and Astroparticle Physics* **2019** (July, 2019) 020, [[1906.11896](#)].
- [9] M. R. Buckley and D. Hooper, *Dark matter subhalos in the Fermi first source catalog*, *Physical Review D* **82** (Sept., 2010) 063501, [[1004.1644](#)].
- [10] M. Ackermann, A. Albert, L. Baldini, J. Ballet, G. Barbiellini, D. Bastieri et al., *Search for Dark Matter Satellites Using Fermi-LAT*, *Astrophysical Journal* **747** (Mar., 2012) 121, [[1201.2691](#)].
- [11] D. Nieto, V. Martínez, N. Mirabal, J. A. Barrio, K. Satalecka, S. Pardo et al., *A search for possible dark matter subhalos as IACT targets in the First Fermi-LAT Source Catalog*, *arXiv e-prints* (Oct., 2011) arXiv:1110.4744, [[1110.4744](#)].
- [12] N. Mirabal, V. Frías-Martínez, T. Hassan and E. Frías-Martínez, *Fermi’s SIBYL: mining the gamma-ray sky for dark matter subhaloes*, *Monthly Notices of the RAS* **424** (July, 2012) L64–L68, [[1205.4825](#)].
- [13] A. V. Belikov, M. R. Buckley and D. Hooper, *Searching for dark matter subhalos in the Fermi-LAT second source catalog*, *Physical Review D* **86** (Aug., 2012) 043504, [[1111.2613](#)].
- [14] H. S. Zechlin, M. V. Fernandes, D. Elsässer and D. Horns, *Dark matter subhaloes as gamma-ray sources and candidates in the first Fermi-LAT catalogue*, *Astronomy and Astrophysics* **538** (Feb., 2012) A93, [[1111.3514](#)].
- [15] A. Berlin and D. Hooper, *Stringent constraints on the dark matter annihilation cross section from subhalo searches with the Fermi Gamma-Ray Space Telescope*, *Physical Review D* **89** (Jan., 2014) 016014, [[1309.0525](#)].
- [16] B. Bertoni, D. Hooper and T. Linden, *Examining The Fermi-LAT Third Source Catalog in search of dark matter subhalos*, *Journal of Cosmology and Astroparticle Physics* **2015** (Dec., 2015) 035, [[1504.02087](#)].
- [17] B. Bertoni, D. Hooper and T. Linden, *Is the gamma-ray source 3FGL J2212.5+0703 a dark matter subhalo?*, *Journal of Cosmology and Astroparticle Physics* **2016** (May, 2016) 049, [[1602.07303](#)].
- [18] N. Mirabal, E. Charles, E. C. Ferrara, P. L. Gonthier, A. K. Harding, M. A. Sánchez-Conde et al., *3FGL Demographics Outside the Galactic Plane using Supervised Machine Learning: Pulsar and Dark Matter Subhalo Interpretations*, *Astrophysical Journal* **825** (July, 2016) 69, [[1605.00711](#)].
- [19] P. M. Saz Parkinson, H. Xu, P. L. H. Yu, D. Salvetti, M. Marelli and A. D. Falcone, *Classification and ranking offermilat gamma-ray sources from the 3fgl catalog using machine learning techniques*, *The Astrophysical Journal* **820** (Mar, 2016) 8.
- [20] R. A. Ibata, G. F. Lewis, M. J. Irwin and T. Quinn, *Uncovering cold dark matter halo substructure with tidal streams*, *Monthly Notices of the RAS* **332** (June, 2002) 915–920, [[astro-ph/0110690](#)].
- [21] K. V. Johnston, D. N. Spergel and C. Haydn, *How Lumpy Is the Milky Way’s Dark Matter Halo?*, *The Astrophysical Journal* **570** (May, 2002) 656–664, [[astro-ph/0111196](#)].
- [22] R. G. Carlberg, *Star Stream Folding by Dark Galactic Subhalos*, *Astrophysical Journal Letters* **705** (Nov., 2009) L223–L226, [[0908.4345](#)].
- [23] J. H. Yoon, K. V. Johnston and D. W. Hogg, *Clumpy Streams from Clumpy Halos: Detecting Missing Satellites with Cold Stellar Structures*, *Astrophysical Journal* **731** (Apr., 2011) 58, [[1012.2884](#)].

- [24] R. G. Carlberg, *Dark Matter Sub-halo Counts via Star Stream Crossings*, *Astrophysical Journal* **748** (Mar., 2012) 20, [[1109.6022](#)].
- [25] R. G. Carlberg, *Modeling GD-1 Gaps in a Milky Way Potential*, *The Astrophysical Journal* **820** (Mar., 2016) 45, [[1512.01620](#)].
- [26] A. Bonaca, C. Conroy, D. W. Hogg, P. A. Cargile, N. Caldwell, R. P. Naidu et al., *High-resolution Spectroscopy of the GD-1 Stellar Stream Localizes the Perturber near the Orbital Plane of Sagittarius*, *Astrophysical Journal Letters* **892** (Apr., 2020) L37, [[2001.07215](#)].
- [27] T. J. L. de Boer, D. Erkal and M. Gieles, *A closer look at the spur, blob, wiggle, and gaps in GD-1*, *MNRAS* **494** (June, 2020) 5315–5332, [[1911.05745](#)].
- [28] S. Abdollahi, F. Acero, M. Ackermann, M. Ajello, W. B. Atwood, M. Axelsson et al., *Fermi Large Area Telescope Fourth Source Catalog*, *Astrophysical Journal, Supplement* **247** (Mar., 2020) 33, [[1902.10045](#)].
- [29] J. Ballet, T. H. Burnett, S. W. Digel and B. Lott, *Fermi Large Area Telescope Fourth Source Catalog Data Release 2*, *arXiv e-prints* (May, 2020) arXiv:2005.11208, [[2005.11208](#)].
- [30] N. V. Chawla, K. W. Bowyer, L. O. Hall and W. P. Kegelmeyer, *SMOTE: Synthetic Minority Over-sampling Technique*, *arXiv e-prints* (June, 2011) arXiv:1106.1813, [[1106.1813](#)].
- [31] L. Breiman, *Machine learning, volume 45, number 1 - springerlink*, *Machine Learning* **45** (10, 2001) 5–32.
- [32] T. Chen and C. Guestrin, *Xgboost: A scalable tree boosting system.*, in *KDD* (B. Krishnapuram, M. Shah, A. J. Smola, C. Aggarwal, D. Shen and R. Rastogi, eds.), pp. 785–794, ACM, 2016.
- [33] C. Gini, *Variabilità e mutabilità*. 1912.
- [34] A. Liaw and M. Wiener, *Classification and regression by randomforest*, *R News* **2** (2002) 18–22.
- [35] M. C. Stroh and A. D. Falcone, *Swift x-ray telescope monitoring of fermi -lat gamma-ray sources of interest*, *The Astrophysical Journal Supplement Series* **207** (Jul, 2013) 28.
- [36] C. O. Heinke, J. A. Tomsick, F. Yusef-Zadeh and J. E. Grindlay, *Two Rapidly Variable Galactic X-ray Transients Observed with Chandra, XMM-Newton, and Suzaku*, *Astrophysical Journal* **701** (Aug., 2009) 1627–1635, [[0906.4743](#)].
- [37] N. Gehrels, *Confidence Limits for Small Numbers of Events in Astrophysical Data*, *Astrophysical Journal* **303** (Apr., 1986) 336.
- [38] P. A. Evans, K. L. Page, J. P. Osborne, A. P. Beardmore, R. Willingale, D. N. Burrows et al., *2SXPS: An Improved and Expanded Swift X-Ray Telescope Point-source Catalog*, *The Astrophysical Journal Supplement Series* **247** (Apr., 2020) 54, [[1911.11710](#)].
- [39] K. V. Johnston, D. N. Spergel and C. Haydn, *How Lumpy Is the Milky Way’s Dark Matter Halo?*, *ApJ* **570** (May, 2002) 656–664, [[astro-ph/0111196](#)].
- [40] R. A. Ibata, G. F. Lewis, M. J. Irwin and T. Quinn, *Uncovering cold dark matter halo substructure with tidal streams*, *MNRAS* **332** (June, 2002) 915–920, [[astro-ph/0110690](#)].
- [41] M. Odenkirchen, E. K. Grebel, C. M. Rockosi, W. Dehnen, R. Ibata, H.-W. Rix et al., *Detection of Massive Tidal Tails around the Globular Cluster Palomar 5 with Sloan Digital Sky Survey Commissioning Data*, *ApJ* **548** (Feb., 2001) L165–L169, [[astro-ph/0012311](#)].
- [42] C. M. Rockosi, M. Odenkirchen, E. K. Grebel, W. Dehnen, K. M. Cudworth, J. E. Gunn et al., *A Matched-Filter Analysis of the Tidal Tails of the Globular Cluster Palomar 5*, *AJ* **124** (July, 2002) 349–363.
- [43] A. H. W. Küpper, P. Kroupa, H. Baumgardt and D. C. Heggie, *Tidal tails of star clusters*, *MNRAS* **401** (Jan., 2010) 105–120, [[0909.2619](#)].

- [44] D. Erkal and V. Belokurov, *Properties of dark subhaloes from gaps in tidal streams*, [\*MNRAS\* \*\*454\*\* \(Dec., 2015\) 3542–3558](#), [[1507.05625](#)].
- [45] D. Erkal, V. Belokurov, J. Bovy and J. L. Sanders, *The number and size of subhalo-induced gaps in stellar streams*, [\*MNRAS\* \*\*463\*\* \(Nov., 2016\) 102–119](#), [[1606.04946](#)].
- [46] R. G. Carlberg, C. J. Grillmair and N. Hetherington, *The Pal 5 Star Stream Gaps*, [\*ApJ\* \*\*760\*\* \(Nov., 2012\) 75](#), [[1209.1741](#)].
- [47] R. G. Carlberg and C. J. Grillmair, *Gaps in the GD-1 Star Stream*, [\*ApJ\* \*\*768\*\* \(May, 2013\) 171](#), [[1303.4342](#)].
- [48] R. A. Ibata, G. F. Lewis and N. F. Martin, *Feeling the Pull: a Study of Natural Galactic Accelerometers. I. Photometry of the Delicate Stellar Stream of the Palomar 5 Globular Cluster*, [\*ApJ\* \*\*819\*\* \(Mar., 2016\) 1](#), [[1512.03054](#)].
- [49] A. M. Price-Whelan and A. Bonaca, *Off the Beaten Path: Gaia Reveals GD-1 Stars outside of the Main Stream*, [\*ApJ\* \*\*863\*\* \(Aug., 2018\) L20](#), [[1805.00425](#)].
- [50] E. Vasiliev, V. Belokurov and D. Erkal, *Tango for three: Sagittarius, LMC, and the Milky Way*, [\*MNRAS\* \*\*501\*\* \(Feb., 2021\) 2279–2304](#), [[2009.10726](#)].
- [51] N. Garavito-Camargo, G. Besla, C. F. P. Laporte, A. M. Price-Whelan, E. C. Cunningham, K. V. Johnston et al., *Quantifying the impact of the Large Magellanic Cloud on the structure of the Milky Way’s dark matter halo using Basis Function Expansions*, *arXiv e-prints* (Oct., 2020) [arXiv:2010.00816](#), [[2010.00816](#)].
- [52] M. I. P. Dierickx and A. Loeb, *Predicted Extension of the Sagittarius Stream to the Milky Way Virial Radius*, [\*ApJ\* \*\*836\*\* \(Feb., 2017\) 92](#), [[1611.00089](#)].
- [53] G. Besla, A. H. G. Peter and N. Garavito-Camargo, *The highest-speed local dark matter particles come from the Large Magellanic Cloud*, [\*J. Cosmology Astropart. Phys.\* \*\*2019\*\* \(Nov., 2019\) 013](#), [[1909.04140](#)].
- [54] R. P. Naidu, C. Conroy, A. Bonaca, B. D. Johnson, Y.-S. Ting, N. Caldwell et al., *Evidence from the H3 Survey That the Stellar Halo Is Entirely Comprised of Substructure*, [\*ApJ\* \*\*901\*\* \(Sept., 2020\) 48](#), [[2006.08625](#)].
- [55] P. Ullio, L. Bergström, J. Edsö and C. Lacey, *Cosmological dark matter annihilations into  $\gamma$  rays: A closer look*, [\*Phys.Rev.D\* \*\*66\*\* \(Dec., 2002\) 123502](#), [[astro-ph/0207125](#)].
- [56] F. Calore, M. Hütten and M. Stref, *Gamma-Ray Sensitivity to Dark Matter Subhalo Modelling at High Latitudes*, [\*Galaxies\* \*\*7\*\* \(Nov., 2019\) 90](#), [[1910.13722](#)].
- [57] E. Charles, M. Sánchez-Conde, B. Anderson, R. Caputo, A. Cuoco, M. Di Mauro et al., *Sensitivity projections for dark matter searches with the fermi large area telescope*, [\*Physics Reports\* \*\*636\*\* \(2016\) 1–46](#).
- [58] M. Hütten, C. Combet, G. Maier and D. Maurin, *Dark matter substructure modelling and sensitivity of the cherenkov telescope array to galactic dark halos*, [\*Journal of Cosmology and Astroparticle Physics\* \*\*2016\*\* \(Sep, 2016\) 047–047](#).
- [59] P. L. Gonthier, A. K. Harding, E. C. Ferrara, S. E. Frederick, V. E. Mohr and Y.-M. Koh, *Population Syntheses of Millisecond Pulsars from the Galactic Disk and Bulge*, [\*Astrophysical Journal\* \*\*863\*\* \(Aug., 2018\) 199](#), [[1806.11215](#)].
- [60] D. A. Smith, P. Bruel, I. Cognard, A. D. Cameron, F. Camilo, S. Dai et al., *Searching a Thousand Radio Pulsars for Gamma-Ray Emission*, [\*The Astrophysical Journal\* \*\*871\*\* \(Jan., 2019\) 78](#), [[1812.00719](#)].
- [61] J. Coronado-Blázquez, M. A. Sánchez-Conde, M. D. Mauro, A. Aguirre-Santaella, I. Ciucă, A. Domínguez et al., *Spectral and spatial analysis of the dark matter subhalo candidates among*



*fermi large area telescope unidentified sources*, *Journal of Cosmology and Astroparticle Physics* **2019** (nov, 2019) 045–045.

- [62] L. Goodenough and D. Hooper, *Possible Evidence For Dark Matter Annihilation In The Inner Milky Way From The Fermi Gamma Ray Space Telescope*, *arXiv e-prints* (Oct., 2009) arXiv:0910.2998, [[0910.2998](#)].
- [63] M. Ajello, A. Albert, W. B. Atwood, G. Barbiellini, D. Bastieri, K. Bechtol et al., *Fermi-LAT Observations of High-Energy Gamma-Ray Emission toward the Galactic Center*, *The Astrophysical Journal* **819** (Mar., 2016) 44, [[1511.02938](#)].



Source name	RA	Dec	P(RF)	P(XGboost)	Initial Detection
4FGL J0003.6+3059	0.9045	30.9898	0.88	0.94	3FGL
4FGL J0048.6−6347	12.1685	−63.7914	0.88	0.91	2FGL
4FGL J0139.5−2228	24.8971	−22.4777	0.54	0.66	4FGL
4FGL J0336.0+7502	54.0249	75.05	0.99	0.99	1FGL
4FGL J0341.9+3153c	55.4852	31.8952	0.85	0.99	2FGL
4FGL J0414.7−4300	63.6977	−43.012	0.90	0.96	4FGL
4FGL J0418.9+6636	64.7254	66.6001	1.00	1.00	2FGL
4FGL J0436.9+2915	69.2464	29.2565	0.72	0.63	4FGL
4FGL J0447.2+2446	71.8014	24.7701	0.98	0.97	4FGL
4FGL J0533.6+5945	83.4175	59.7622	0.98	0.97	3FGL
4FGL J0545.7+6016	86.4419	60.2704	0.95	0.99	1FGL
4FGL J0802.1−5612	120.5456	−56.2012	1.00	0.99	1FGL
4FGL J0906.8−2122	136.7046	−21.3724	0.66	0.84	4FGL
4FGL J0940.3−7610	145.0989	−76.1794	0.99	0.96	1FGL
4FGL J0953.6−1509	148.4055	−15.1549	0.99	0.99	1FGL
4FGL J1106.7−1742	166.699	−17.7148	0.83	0.68	1FGL
4FGL J1120.0−2204	170.0016	−22.0779	0.99	0.96	1FGL
4FGL J1126.0−5007	171.5145	−50.1194	0.74	0.69	3FGL
4FGL J1204.5−5032	181.1483	−50.5456	0.98	0.91	4FGL
4FGL J1207.4−4536	181.8734	−45.6125	0.99	0.88	3FGL
4FGL J1225.9+2951	186.4902	29.8596	1.00	0.97	1FGL
4FGL J1231.6−5116	187.9102	−51.2672	0.99	0.99	1FGL
4FGL J1345.9−2612	206.4815	−26.2116	0.87	0.63	2FGL
4FGL J1400.0−2415	210.0206	−24.266	0.94	0.99	2FGL
4FGL J1429.8−0739	217.4512	−7.6506	0.52	0.69	4FGL
4FGL J1458.8−2120	224.7033	−21.3388	0.85	0.99	2FGL
4FGL J1526.6−2743	231.6709	−27.7327	1.00	0.98	4FGL
4FGL J1526.6−3810	231.6594	−38.169	0.99	0.99	3FGL
4FGL J1527.8+1013	231.9709	10.2286	0.91	0.93	4FGL
4FGL J1530.0−1522	232.5011	−15.3759	0.96	0.98	4FGL
4FGL J1539.4−3323	234.8511	−33.3987	0.85	0.99	1FGL
4FGL J1543.6−0244	235.9077	−2.7471	0.96	0.56	1FGL
4FGL J1544.2−2554	236.0523	−25.9125	1.00	0.98	2FGL
4FGL J1602.2+2305	240.5576	23.0969	0.93	0.99	2FGL
4FGL J1612.1+1407	243.0313	14.1168	0.90	0.99	2FGL
4FGL J1622.2−7202	245.5525	−72.0399	0.89	0.99	4FGL
4FGL J1623.9−6936	245.9865	−69.6069	0.81	0.87	4FGL
4FGL J1630.1−1049	247.5289	−10.8183	0.99	0.74	1FGL
4FGL J1646.7−2154	251.6851	−21.9075	0.97	0.98	4FGL
4FGL J1656.4−0410	254.1194	−4.1702	0.78	0.99	4FGL
4FGL J1659.0−0140	254.7655	−1.6775	0.75	0.99	2FGL
4FGL J1700.0−0122	255.0191	−1.3734	0.82	0.70	4FGL
4FGL J1709.9−0900	257.4834	−9.0144	0.96	0.99	4FGL
4FGL J1711.9−1922	257.9776	−19.3676	0.96	0.99	4FGL

4FGL J1717.5−5804	259.3784	−58.0706	0.98	0.92	2FGL
4FGL J1720.6+0708	260.1638	7.1469	0.99	0.65	1FGL
4FGL J1722.8−0418	260.7115	−4.3033	0.72	0.74	1FGL
4FGL J1730.4−0359	262.6086	−3.9923	1.00	0.99	1FGL
4FGL J1757.7−6032	269.4489	−60.5374	0.88	0.96	2FGL
4FGL J1813.5+2819	273.3922	28.3263	0.56	0.80	3FGL
4FGL J1818.6+1316	274.6527	13.2731	0.94	0.65	3FGL
4FGL J1823.2+1209	275.8120	12.1573	0.97	0.99	4FGL
4FGL J1824.2−5427	276.0704	−54.4514	0.91	0.73	3FGL
4FGL J1827.5+1141	276.8786	11.6863	0.99	0.98	2FGL
4FGL J1831.1−6503	277.7773	−65.0659	0.99	0.99	1FGL
4FGL J1842.1+2737	280.5378	27.6248	0.93	0.61	2FGL
4FGL J1845.8−2521	281.4648	−25.3585	0.99	0.78	3FGL
4FGL J1855.6−3603	283.9149	−36.0611	0.97	0.78	4FGL
4FGL J1858.3−5424	284.576	−54.4123	0.91	0.82	3FGL
4FGL J1906.4−1757	286.6107	−17.9509	0.71	0.99	4FGL
4FGL J1910.7−5320	287.6989	−53.3385	0.83	0.94	1FGL
4FGL J1913.4−1526	288.3515	−15.4496	0.97	0.85	4FGL
4FGL J1920.0−2622	290.023	−26.3775	0.52	0.52	4FGL
4FGL J1924.8−1035	291.2053	−10.5909	1.00	1.00	2FGL
4FGL J1949.2−1453	297.3162	−14.8983	0.74	0.54	2FGL
4FGL J2026.3+1431	306.5988	14.5225	0.74	0.79	3FGL
4FGL J2029.5−4237	307.3765	−42.6285	0.91	0.74	3FGL
4FGL J2043.9−4802	310.9815	−48.0398	0.95	0.98	2FGL
4FGL J2112.5−3043	318.1400	−30.7293	0.96	0.99	1FGL
4FGL J2133.1−6432	323.2951	−64.5383	1.00	0.99	1FGL
4FGL J2212.4+0708	333.1083	7.1428	0.99	0.92	1FGL
4FGL J2219.7−6837	334.9469	−68.6173	0.61	0.93	3FGL
4FGL J2250.5+3305	342.6404	33.0989	0.97	0.99	3FGL

**Table 1:** Subhalo candidates in the 4FGL-DR2

Source name	$N_H$ (cm <sup>2</sup> )	X-ray Flux Upper Limit (erg cm <sup>-2</sup> s <sup>-1</sup> )
4FGL J0003.6+3059	$4.9 \times 10^{20}$	$1.5 \times 10^{-13}$ (PS)
4FGL J0048.6-6347	$2.2 \times 10^{20}$	$< 8.4 \times 10^{-14}$
4FGL J0139.5-2228	$9.9 \times 10^{19}$	$< 8.9 \times 10^{-14}$
4FGL J0336.0+7502	$1.5 \times 10^{21}$	$4.5 \times 10^{-14}$ (PS)
4FGL J0341.9+3153c	$1.2 \times 10^{21}$	$8.6 \times 10^{-13}$ (PS)
4FGL J0436.9+2915	$1.7 \times 10^{21}$	$< 1.6 \times 10^{-13}$
4FGL J0447.2+2446	$2.1 \times 10^{21}$	$< 8.6 \times 10^{-13}$
4FGL J0533.6+5945	$1.8 \times 10^{21}$	$< 1.2 \times 10^{-13}$
4FGL J0545.7+6016	$1.5 \times 10^{21}$	$< 2.0 \times 10^{-13}$
4FGL J0802.1-5612	$1.4 \times 10^{21}$	$4.1 \times 10^{-14}$ (PS)
4FGL J0906.8-2122	$1.1 \times 10^{21}$	$< 8.1 \times 10^{-14}$
4FGL J0940.3-7610	$9.6 \times 10^{20}$	$2.2 \times 10^{-13}$ (PS)
4FGL J0953.6-1509	$5.8 \times 10^{20}$	$< 7.7 \times 10^{-14}$
4FGL J1106.7-1742	$4.0 \times 10^{20}$	Partially Covered
4FGL J1120.0-2204	$4.1 \times 10^{20}$	$7.2 \times 10^{-14}$ (PS)
4FGL J1126.0-5007	$9.1 \times 10^{20}$	$6.2 \times 10^{-14}$ (PS) (also GRB 140719A in error ellipse)
4FGL J1204.5-5032	$1.1 \times 10^{21}$	$< 7.5 \times 10^{-14}$
4FGL J1207.4-4536	$6.7 \times 10^{20}$	$2.8 \times 10^{-13}$ (PS)
4FGL J1225.9+2951	$1.6 \times 10^{20}$	$< 8.7 \times 10^{-14}$
4FGL J1231.6-5116	$1.4 \times 10^{21}$	$< 1.2 \times 10^{-13}$
4FGL J1345.9-2612	$4.7 \times 10^{20}$	$< 8.6 \times 10^{-14}$
4FGL J1400.0-2415	$5.1 \times 10^{20}$	$< 6.4 \times 10^{-14}$
4FGL J1429.8-0739	$4.6 \times 10^{20}$	$8.5 \times 10^{-13}$ (PS)
4FGL J1458.8-2120	$7.4 \times 10^{20}$	$< 8.3 \times 10^{-14}$
4FGL J1526.6-3810	$1.0 \times 10^{21}$	$< 1.4 \times 10^{-13}$
4FGL J1526.6-2743	$7.7 \times 10^{20}$	$< 1.4 \times 10^{-13}$
4FGL J1527.8+1013	$2.8 \times 10^{20}$	$1.1 \times 10^{-13}$ (PS)
4FGL J1530.0-1522	$8.3 \times 10^{20}$	$1.4 \times 10^{-13}$ (PS)
4FGL J1539.4-3323	$9.0 \times 10^{20}$	$< 9.0 \times 10^{-15}$
4FGL J1543.6-0244	$7.9 \times 10^{20}$	$< 9.6 \times 10^{-14}$
4FGL J1544.2-2554	$1.1 \times 10^{21}$	$< 9.9 \times 10^{-14}$
4FGL J1602.2+2305	$4.3 \times 10^{20}$	$< 1.2 \times 10^{-13}$
4FGL J1612.1+1407	$3.1 \times 10^{20}$	$< 8.4 \times 10^{-14}$
4FGL J1622.2-7202	$7.5 \times 10^{20}$	$8.9 \times 10^{-14}$ (PS)
4FGL J1623.9-6936	$9.7 \times 10^{20}$	$< 7.7 \times 10^{-14}$
4FGL J1627.7-5749	$2.7 \times 10^{21}$	Partially Covered
4FGL J1630.1-1049	$1.3 \times 10^{21}$	$< 1.1 \times 10^{-13}$
4FGL J1646.7-2154	$1.3 \times 10^{21}$	Not Covered
4FGL J1656.4-0410	$1.0 \times 10^{21}$	$1.2 \times 10^{-13}$ (PS)
4FGL J1659.0-0140	$8.4 \times 10^{20}$	$< 1.3 \times 10^{-13}$
4FGL J1700.0-0122	$8.5 \times 10^{20}$	$2.6 \times 10^{-13}$ (PS)
4FGL J1709.9-0900	$1.5 \times 10^{21}$	$< 1.1 \times 10^{-13}$
4FGL J1711.9-1922	$1.5 \times 10^{21}$	$< 1.9 \times 10^{-13}$
4FGL J1717.5-5804	$9.2 \times 10^{20}$	$< 2.6 \times 10^{-13}$

4FGL J1720.6+0708	$6.2 \times 10^{20}$	$< 1.0 \times 10^{-13}$
4FGL J1722.8-0418	$1.3 \times 10^{21}$	$< 1.0 \times 10^{-13}$
4FGL J1730.4-0359	$1.5 \times 10^{21}$	$< 9.0 \times 10^{-13}$
4FGL J1757.7-6032	$6.8 \times 10^{20}$	$< 1.2 \times 10^{-13}$
4FGL J1813.5+2819	$7.4 \times 10^{20}$	$< 1.2 \times 10^{-13}$
4FGL J1818.6+1316	$9.8 \times 10^{20}$	$< 1.2 \times 10^{-13}$
4FGL J1823.2+1209	$1.3 \times 10^{21}$	$< 1.3 \times 10^{-13}$
4FGL J1824.2-5427	$7.7 \times 10^{20}$	$< 1.3 \times 10^{-13}$
4FGL J1827.5+1141	$1.4 \times 10^{21}$	$< 1.1 \times 10^{-13}$
4FGL J1831.1-6503	$6.1 \times 10^{20}$	$< 1.1 \times 10^{-13}$
4FGL J1842.1+2737	$1.1 \times 10^{21}$	$< 1.1 \times 10^{-13}$
4FGL J1845.8-2521	$1.2 \times 10^{21}$	$< 1.3 \times 10^{-13}$
4FGL J1855.6-3603	$6.4 \times 10^{20}$	$< 1.4 \times 10^{-13}$
4FGL J1858.3-5424	$6.0 \times 10^{20}$	$< 1.8 \times 10^{-13}$
4FGL J1906.4-1757	$9.1 \times 10^{20}$	Not covered
4FGL J1910.7-5320	$5.3 \times 10^{20}$	$< 3.3 \times 10^{-13}$
4FGL J1920.0-2622	$7.9 \times 10^{20}$	$< 1.2 \times 10^{-13}$
4FGL J1924.8-1035	$1.2 \times 10^{21}$	$< 1.1 \times 10^{-13}$
4FGL J1949.2-1453	$7.8 \times 10^{20}$	$< 1.1 \times 10^{-13}$
4FGL J2026.3+1431	$6.2 \times 10^{20}$	$< 1.0 \times 10^{-13}$
4FGL J2029.5-4237	$3.7 \times 10^{20}$	$3.7 \times 10^{-13}(\text{PS})$
4FGL J2043.9-4802	$2.7 \times 10^{20}$	$< 5.2 \times 10^{-14}$
4FGL J2112.5-3043	$6.4 \times 10^{20}$	$< 2.5 \times 10^{-14}$
4FGL J2133.1-6432	$3.2 \times 10^{20}$	$< 6.0 \times 10^{-14}$
4FGL J2212.4+0708	$6.2 \times 10^{20}$	$1.3 \times 10^{-13}(\text{PS})$
4FGL J2219.7-6837	$2.8 \times 10^{20}$	$< 1.5 \times 10^{-13}$
4FGL J2250.5+3305	$8.0 \times 10^{20}$	$2.0 \times 10^{-13}(\text{PS})$

**Table 2:** X-ray upper limits for 4FGL-DR2 subhalo candidates. PS denotes at least one X-ray point source within the LAT error ellipse. Partial or no *Swift* coverage are also indicated.